International Journal of Mechanical Sciences 57 (2012) 74–78

Contents lists available at SciVerse ScienceDirect

International Journal of Mechanical Sciences

journal homepage: www.elsevier.com/locate/ijmecsci

The calculation of roll torque and roll separating force for broadside rolling by stream function method

S.H. Zhang *, D.W. Zhao, C.R. Gao

State Key Lab of Rolling and Automation, Northeastern University, Shenyang 110819, China

ARTICLE INFO

Article history:
Received 8 November 2011
Received in revised form
14 February 2012
Accepted 17 February 2012
Available online 22 February 2012

Keywords:
Broadside rolling
Roll separating force
Strain rate vector
Stream function
Analytical solution

ABSTRACT

A two-dimensional velocity field for broadside rolling is proposed by reducing the dual-stream function velocity field. By using the field and the strain vector inner product, an analytical solution of roll torque and separating force for broadside rolling is first obtained. The theoretical predictions of roll torque and separating force are compared with actual measured data. The result reveals that the proposed solution is appropriate for solving broadside rolling, and the roll torque and separating force are in good agreement with the actual measured ones since the maximum errors are less than 15%. Moreover, the effects of various rolling conditions such as thickness reduction, friction factor and shape factor, upon separating force, location of neutral angle, and stress state coefficient are discussed systematically.

1. Introduction

Accurate determination of the roll torque and separating force is a major issue in the flat rolling. It is the basis for planning and controlling of the production process. A numerical solution with Ritz approximation was ever given by Oh and Kobayashi, and finite element method given by many researchers [1–3], analytical solution for plate rolling has not been reported yet till now. The finite element method, FEM, was extensively used by many researchers to simulate two-and three-dimensional metal flow. Park and Oh [4] developed a rigid-plastic 3D FEM code for the analysis of shape rolling processes, which is capable of handing arbitrary cross-sections. Kim et al. [5] combined the two-dimensional rigid-plastic finite element method with the slab method to reduce the amount of computation without losing accuracy. A 2D plane strain finite element model of flat-rolling process was presented by Dvorkin et al. and the correction to slipping and bending of the rolled plate was demonstrated [6]. But the large computation times and memory capacities used during modeling are the disadvantages of FEM method, especially for personal computers. Abrinia and Fazlirad pointed that obtaining a full analytical solution for the roll torque and separating force has been one of the most difficult problems in the analysis of plate rolling because of the difficulties in formulating the governing equation [7]. Moreover, few attempts have been reported to predict the broadside rolling force in the extra-thick plate mill since the contact arc-to-height ratio (called shape factor) usually is less than 1 and the width-to-height ratio is larger than 10. However, the accurate roll torque and roll separating force for broadside rolling in a roughing sequence are the prerequisite for the automatic control of the rolling mill [8,9].

Motivated by the information above, the present paper proposes an analytical solution to the total power functional for broadside rolling. The idea of the proposed model is to reduce a three-dimensional problem to a two-dimensional one considering the deformation characteristics during broadside rolling. The validity of the model has been examined by comparing the calculated results with the measured ones for some domestic plant in one rolling mill. Comparison shows that the theoretical predictions of roll torque and roll separating force are in good agreement with the experimental measurements. In addition, the effects of thickness reduction, friction factor, and shape factor on the location of neutral point, and stress state coefficient are discussed.

2. Theoretical analysis

2.1. Velocity field for broadside rolling

In the reversing roughing mill, the broadside rolling passes are usually carried out after the initial-sizing rolling, that is, the slab is first turned 90 degrees and rolled in the transverse direction. So for those passes although $l/h \leq 1$, the width-to-height ratio b/h is

* Correspondence author. Tel.: +86 24 83680570; fax: +86 24 23906472.
E-mail address: zhangshunhusci@yahoo.cn (S.H. Zhang).

0020-7403/$ - see front matter © 2012 Elsevier Ltd. All rights reserved.
doi:10.1016/j.ijmecsci.2012.02.006

Nomenclature

h_x,h_m	half of the plate thickness and half of the average plate thickness in the roll gap
h_0,h_1	half of the initial and final plate thickness at inlet and outlet, respectively
h'_x,h''_x	the first and second order derivatives of h_x
h	plate thickness
l	contact length
b	plate width
θ	bite angle
σ_s	yield stress
k	yield shear stress
v_x,v_y,v_z	velocity components in x, y, z directions
$\overline{\sigma}$	equivalent flow stress
$\dot{\varepsilon}_{ij}$,$\dot{\bar{\varepsilon}}_{ij}$	strain rates and equivalent strain rate
Δh	half of the absolute reduction
ε_3	relative reduction
v_R	roll circumferential velocity
τ_f	frictional shear stress on the plate surface
Δv_f	discontinuous quantity of tangential velocity
v_0	inlet velocity of plate
α,β,γ	direction angles formed by τ_f and the coordinate axes in x, y, z directions, respectively
N_d	internal strain energy rate
N_f	friction energy rate
N_s	shear energy rate
U	flow volume per second of the deformation part
α_n	neutral angle
Φ	total power
$M_{\min}$	minimum value of roll torque
$F_{\min}$	minimum value of separating force
n_σ	stress state coefficient
m	friction factor
χ	lever arm ratio

usually larger than 10 and the spread in longitudinal direction of the slab is certainly negligible.

An initial plate with thickness of $2h_0$ was rolled into a final thickness of $2h_1$ through a pair of rolls in the investigated process. The axes of Cartesian coordinate system are chosen and their origin is located at the center of inlet section of deformation zone, as shown in Fig. 1.

In the present paper, the roll is taken to be rigid and the effect of roll flattening on the roll torque and roll separating force is not considered. From the geometry, the contact arc, parametric and the first and second order derivative equations presented by Zhao are as follows [10]:

$$\left.\begin{aligned} z = h_x = R + h_1 - [R^2 - (l-x)^2]^{1/2} \\ z = h_\alpha = R + h_1 - R\cos\alpha \end{aligned}\right\} \tag{1}$$

$$l - x = R\sin\alpha, \quad \mathrm{d}x = -R\cos\alpha\,\mathrm{d}\alpha, \tag{2}$$

$$h'_x = -\tan\alpha, \quad h''_x = (R\cos^3\alpha)^{-1} \tag{3}$$

where R is radius of the roller.

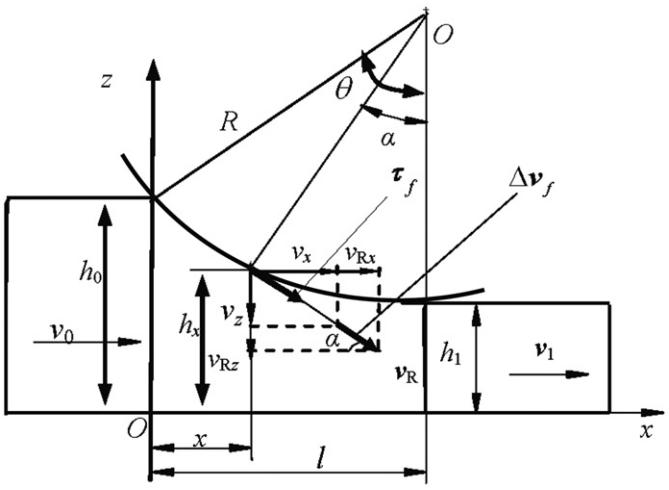

Fig. 1. Deformation zone in plate rolling.

According to Fig. 1, the geometrical boundary conditions are written as

$$\begin{aligned} &x = 0, \quad \alpha = \theta, \quad h_x = h_\alpha = h_\theta = h_0; \quad h'_x = -\tan\theta \\ &x = l, \quad \alpha = 0, \quad h_x = h_\alpha = h_1; \quad h'_x = 0. \end{aligned} \tag{4}$$

For broadside rolling, $l/h < 1, b/h \gg 10$, the b_x from the entry to exit can be taken as a constant, therefore

$$y = b_x = b_1 = b_0 = b \tag{5}$$

According to the three-dimensional rolling field proposed by Oh and Kobayashi [1], a two-dimensional velocity field and the strain rate components are determined by setting the proportional factor in Kobayashi velocity to 1. The velocity components are as follows:

$$v_x = \frac{U}{h_x b}, \quad v_z = v_x \frac{h'_x}{h_x} z, \quad v_y = 0 \tag{6}$$

$$U = v_x h_x b = v_n h_n b = v_R \cos\alpha_n b(R + h_1 - R\cos\alpha_n) = v_1 h_1 b \tag{7}$$

$$\begin{aligned} &\dot{\varepsilon}_x = -v_x \frac{h'_x}{h_x}, \ \dot{\varepsilon}_z = v_x \frac{h'_x}{h_x}, \\ &\dot{\varepsilon}_{xz} = \frac{z}{2} v_x \left[\frac{h''_x}{h_x} - 2\left(\frac{h'_x}{h_x}\right)^2\right], \\ &\dot{\varepsilon}_{xy} = \dot{\varepsilon}_{yz} = 0. \end{aligned} \tag{8}$$

where U is the flow volume per second of the deformation part.

Eq. (6) indicates that the three-dimensional velocity field proposed by Kobayashi is reduced to a two-dimensional one. In Eqs. (6) and (8), $\dot{\varepsilon}_x + \dot{\varepsilon}_z = 0$; $x=0$, $v_x = v_0$; $x=l$, $v_x = v_1$; $z=0$, $v_z = 0$; $z=h_x$, $v_z = -v_x\tan\alpha$. So, they are also kinematically admissible.

2.2. Internal strain energy rate

The internal strain energy rate N_d of deformation dissipated in the plastic region can be calculated with the equivalent strain rate and the equivalent flow stress $\overline{\sigma}$ of the deformed material

$$N_d = \iiint_V \overline{\sigma}\dot{\bar{\varepsilon}}\,\mathrm{d}V = 4\sqrt{\frac{2}{3}}\sigma_s \int_0^{h_x}\int_0^{l} v_x \sqrt{g^2 + I^2 z^2}\, b\,\mathrm{d}x\mathrm{d}z \tag{10}$$

$$g = \sqrt{2}h'_x/h_x, \quad I = [h''_x/h_x - 2(h'_x/h_x)^2]/\sqrt{2}. \tag{11}$$

Notice that in Eq. (11) g and I are monodrome functions of x, so the integral mean value theorem can be applied

$$\overline{\frac{h_x'}{h_x}}=\frac{1}{l}\int_0^l\frac{h_x'}{h_x}\mathrm{d}x=-\frac{\ln(h_0/h_1)}{l}=-\frac{\varepsilon_3}{l}\approx-\frac{\Delta h}{lh_0}.$$

$$\overline{h_x'}=\frac{1}{l}\int_0^l h_x'\mathrm{d}x=-\frac{\Delta h}{l};$$

$$\therefore\ \frac{\overline{h_x''}}{\overline{h_x}}=\frac{\overline{h_x''}}{h_m}=\frac{1}{lh_m}\int_0^l\mathrm{d}h_x'=\frac{1}{lh_m}h_x'|_0^l=\frac{\tan\theta}{lh_m}\approx\frac{2\Delta h}{l^2h_m};$$

Substituting $\varepsilon_3=\Delta h/h_0$ into Eq. (11) leads to

$$g=-\frac{\sqrt{2}\varepsilon_3}{l},\quad I=\frac{\sqrt{2}}{l^2}\left(\frac{\Delta h}{h_m}-\varepsilon_3^2\right)\tag{12}$$

Here, a new integration method called strain rate vector inner-product method is introduced, as proposed by Zhao et al. [11–13]. The main idea of the new integration method can be briefly generalized as: transforming strain rate tensor to strain rate vector; integrating each inner-product item of strain rate vector; summing all the integral items.

Substituting strain rate vector $\dot{\boldsymbol{\varepsilon}}=gv_x\boldsymbol{i}+Izv_x\boldsymbol{k}$ and unit vector $\dot{\boldsymbol{\varepsilon}}_0=l_1\boldsymbol{i}+l_3\boldsymbol{k}$ into Eq. (10), then

$$\begin{aligned}N_d&=4\sqrt{\frac{2}{3}}\sigma_s\int_0^l\int_0^{h_x}\dot{\varepsilon}\cdot\dot{\varepsilon}_0b\mathrm{d}x\mathrm{d}z\\&=4b\sqrt{\frac{2}{3}}\sigma_s\int_0^l\int_0^{h_x}(gv_x\cos\alpha+Izv_x\cos\gamma)\mathrm{d}x\mathrm{d}z\\&=4b\sqrt{\frac{2}{3}}\sigma_s\int_0^l\int_0^{h_x}\left[\frac{gv_x\mathrm{d}x\mathrm{d}z}{\sqrt{1+(\mathrm{d}z/\mathrm{d}x)^2}}+\frac{Izv_x\mathrm{d}x\mathrm{d}z}{\sqrt{1+(\mathrm{d}x/\mathrm{d}z)^2}}\right]\end{aligned}\tag{13}$$

where $l_1=\cos\alpha$, $l_3=\cos\gamma$are projections of unit vector on the coordinate axis.

From Eq. (6), we have

$$\mathrm{d}z/\mathrm{d}x=[v_z/v_x]_{z=h_x}=h_x'=-\tan\theta\approx2\Delta h/l,\mathrm{d}x/\mathrm{d}z=1/h_x'=-l/2\Delta h$$

Substituting $\mathrm{d}z/\mathrm{d}x$ and $\mathrm{d}x/\mathrm{d}z$ into Eq. (13) and noticing Eq. (12), the termwise integration becomes:

$$\begin{aligned}I_1&=\int_0^l\int_0^{h_x}\frac{gv_x\mathrm{d}x\mathrm{d}z}{\sqrt{1+(h_x')^2}}=\frac{U}{b}\frac{\sqrt{2}\varepsilon_3}{\sqrt{1+(2\Delta h/l)^2}}\frac{\int_0^l\mathrm{d}x}{l}\\&=\frac{\sqrt{2}lU}{b}f_1,f_1=\frac{\varepsilon_3}{\sqrt{l^2+4\Delta h^2}}.\end{aligned}\tag{14}$$

$$\begin{aligned}I_3&=\frac{Ul\sqrt{2}(2\Delta h^2/h_m-2\Delta h\varepsilon_3^2)h_m}{2bl^2\sqrt{l^2+4\Delta h^2}}\\&=\frac{\sqrt{2}lU}{b}f_3,f_3=\frac{(2\Delta h^2-2\Delta hh_m\varepsilon_3^2)}{2l^2\sqrt{l^2+4\Delta h^2}}.\end{aligned}\tag{15}$$

Substituting Eqs. (14) and (15) into Eq. (13), the N_d is as follows

$$N_d=\frac{8\sigma_slU}{\sqrt{3}}(f_1+f_3)\tag{16}$$

where $l=\sqrt{2R\Delta h}$, $\Delta h=h_0-h_1$, $h_m=(h_0+2h_1)/3$, $\varepsilon_3=\Delta h/h_0$, $b=(b_0+b_1)/2$

2.3. Friction energy rate

The friction energy rate at the interface between the roller and the work piece is:

$$N_f=\frac{4\sigma_smb}{\sqrt{3}}\int_0^l\Delta v_f\sqrt{1+h_x'^2}\mathrm{d}x,$$

$$\Delta v_f=v_R-v_x\sqrt{1+h_x'^2}=v_R-v_x\sec\alpha\tag{17}$$

The roll surface equation is

$$z=h_x=R+h_1-[R^2-(l-x)^2]^{1/2},\quad \mathrm{d}F=\sqrt{1+(h_x')^2}b\mathrm{d}x,b\sec\alpha$$

The concrete solution of co-line vector inner for friction energy rate is

$$\begin{aligned}N_f&=4\int_0^l\boldsymbol{\tau}_f\cdot\Delta\boldsymbol{v}_f\mathrm{d}F\\&=4\int_0^l(\tau_{fx}\Delta v_x+\tau_{fz}\Delta v_z)\sqrt{1+(h_x')^2}b\mathrm{d}x\\&=4mkb\int_0^l(\Delta v_x\cos\alpha+\Delta v_z\cos\gamma)\sec\alpha\mathrm{d}x\end{aligned}\tag{18}$$

From Fig. 1, the direction cosines formed by the intersecting angles of Δv_f (or $\tau_f=mk$) and the coordinate axes are, respectively

$$\begin{aligned}&\cos\alpha=\pm\sqrt{R^2-(l-x)^2}/R,\\&\cos\gamma=\pm(l-x)/R=\sin\alpha,\cos\beta=0.\end{aligned}\tag{19}$$

Taking notice of Eq. (2), substituting Eq. (19) into Eq. (18) yields

$$\begin{aligned}N_f&=4mkb\left[\int_0^l\cos\alpha(v_R\cos\alpha-v_x)\sec\alpha\mathrm{d}x\right.\\&\quad\left.+\int_0^l\sin\alpha(v_R\sin\alpha-v_x\tan\alpha)\sec\alpha\mathrm{d}x\right]\\&=4mkb(\mathrm{I}_1,I_2)\end{aligned}$$

$$\begin{aligned}I_1&=\int_0^l(v_R\cos\alpha-v_x)dx=\int_0^{x_n}(v_R\cos\alpha-v_x)dx-\int_{x_n}^l(v_R\cos\alpha-v_x)\mathrm{d}x\\&=v_RR\left(\frac{\theta}{2}-\alpha_\mathrm{n}+\frac{\sin2\theta}{4}-\frac{\sin2\alpha_\mathrm{n}}{2}\right),\frac{U(l-2x_n)}{bh_m}\end{aligned}$$

$$\begin{aligned}I_2&=\int_0^{x_n}(v_R\sin\alpha-v_x\tan\alpha)\tan\alpha\mathrm{d}x-\int_{x_n}^l(v_R\sin\alpha-v_x\tan\alpha)\tan\alpha\mathrm{d}x\\&=v_RR\left(\frac{\theta}{2}-\alpha_n+\frac{\sin2\alpha_n}{2}-\frac{\sin2\theta}{4}\right)+\frac{UR}{bh_m}\left[2ln\tan\left(\frac{\pi}{4}+\frac{\alpha_n}{2}\right)\right.\\&\quad\left.-\ln\tan\left(\frac{\pi}{4}+\frac{\theta}{2}\right)\right]+\frac{U(2x_n-l)}{bh_m}\end{aligned}$$

$$N_f=4mkb(I_1+I_2)=4mkb\left[v_RR(\theta-2\alpha_n)+\frac{UR}{bh_m}\ln\frac{\tan^2((\pi/4)+(\alpha_n/2))}{\tan((\pi/4)+(\theta/2))}\right]\tag{20}$$

where subscript n denotes the neutral point in variables α_n and x_n.

2.4. Shear energy rate

From Eq. (6), $x=l,h_x'=b_x'=0$; $v_y|_{x=l}=\mathrm{v}_z|_{x=l}=0$; so, on the exit section no shear energy rate is dissipated but on the entry section:

$$|\Delta v_z|_{x,0}=|0-\overline{v}_z|_{x=0}|=\overline{v}_z|_{x,0}=v_0\frac{\overline{h_x'}}{\overline{h}_x}z=-\frac{v_0\varepsilon_3}{l}z,\tag{21}$$

$$\begin{aligned}N_s&=N_{s0}=4\int_0^{h_0}k|\Delta v_z|b\mathrm{d}z=4k\int_0^{h_0}\frac{v_0\varepsilon_3}{l}zb\mathrm{d}z=2klU\frac{h_0\varepsilon_3}{l^2}\\&=2klUf_4,f_4=\frac{\Delta h}{l^2}.\end{aligned}\tag{22}$$

where θ is called the bite angle and $k=\sigma_s/\sqrt{3}$ the yield shear stress.

2.5. The total power and its minimization

The total power Φ is obtained as follows:

$$\Phi = N_d + N_f + N_s \tag{23}$$

Sum of Eqs. (16), (20) and (22) yields the analytical solution of total energy rate as follows

$$\Phi = \frac{8\sigma_s lU}{\sqrt{3}}\left(f_1 + f_3 + \frac{f_4}{4}\right) + \frac{4m\sigma_s}{\sqrt{3}}\left[bv_R R(\theta - 2\alpha_n) + \frac{UR}{h_m}\ln\frac{\tan^2((\pi/4)+(\alpha_n/2))}{\tan((\pi/4)+(\theta/2))}\right] \tag{24}$$

where v_R is the roll circumferential velocity, α_n is the neutral angle.

From Eq. (7), Eqs. (16), (20) and (22), we have

$$dU/d\alpha_n = v_R bR\sin 2\alpha_n - v_R b(R+h_1)\sin\alpha_n = N, \tag{25}$$

$$\frac{\partial N_d}{\partial \alpha_n} = Nl\frac{8\sigma_s}{\sqrt{3}}(f_1 + f_3), \frac{\partial N_{s0}}{\partial \alpha_n} = Nl\frac{2\sigma_s}{\sqrt{3}}f_4, \tag{26}$$

$$\frac{\partial N_f}{\partial \alpha_n} = \frac{4m\sigma_s}{\sqrt{3}}\left[\frac{2UR}{h_m\cos\alpha_n} - 2v_R bR + \frac{NR}{h_m}\ln\frac{\tan^2((\pi/4)+(\alpha_n/2))}{\tan((\pi/4)+(\theta/2))}\right] \tag{27}$$

Differentiation of Eq. (24) with respect to α_n yields the equation as follows:

$$\frac{d\Phi}{d\alpha_n} = \frac{\partial N_d}{\partial \alpha_n} + \frac{\partial N_{s0}}{\partial \alpha_n} + \frac{\partial N_f}{\partial \alpha_n} = 0 \tag{28}$$

Solving Eq. (28), the expression of m can be obtained as follows:

$$m = Nl\left(f_1 + f_3 + \frac{f_4}{4}\right)\Big/\left\{v_R bR - \frac{UR}{h_m\cos\alpha_n} - \frac{NR}{2h_m}\ln\frac{\tan^2((\pi/4)+(\alpha_n/2))}{\tan((\pi/4)+(\theta/2))}\right\} \tag{29}$$

It can be seen that the friction factor is a function of the reduction, roll speed, roll radius, plate width, rolled plate thickness, and neutral angel.

Substituting Eq. (29) into Eq. (24), then one can get the minimum of total energy rate $\Phi_{\min}$ for various friction conditions. So, the minimum values of roll torque, separating force and stress state coefficient can be calculated as follows:

$$M_{\min} = \frac{R}{2v_R}\Phi_{\min},\ F_{\min} = \frac{M_{\min}}{\chi\cdot\sqrt{2R\Delta h}},\quad n_\sigma = \frac{F_{\min}}{4blk}, \tag{30}$$

where the lever arm ratio χ can refer to the research result, as given by Ref. [14]. The χ is about 0.5 for hot rolling and 0.45 for cold rolling.

3. Experimental work

Deformation is implemented by using a rolling mill which was built in a domestic factory. The work roll of the mill has a diameter of 1070 mm. The thickness of $320\times1800\times3650$ (mm^3) cast slab is reduced to 303 mm in initial-sizing rolling (the No. 1 pass). Then the slab is rolled subsequently until all rough rolling passes are conducted. It is noted that those passes from No. 2 to No. 9 belong to weak plane strain rolling since their ratios of width to height are bigger than 10. The roll speeds from No.2 to No. 9 pass are 1.24, 1.64, 1.26, 1.66, 1.30, 1.86, 1.81, and 2.11 m/s, respectively. The χ for No. 2 to No. 9 pass are 0.49, 0.51, 0.50, 0.49, 0.50, 0.51, 0.55 and 0.55, respectively. The corresponding rolling temperatures are 900, 886, 879, 872, 872, 878, 881 and 891. The exit thickness is measured directly after each pass and the roll separating force is monitored. The material used in the experiment is E355CC (ISO) steel and its deformation resistance model determined by Chen et al. [15] is as follows:

$$\sigma_s = 6310.7\varepsilon^{0.407}\dot{\varepsilon}^{0.115}\exp(-2.62\times10^{-3}T - 0.669\varepsilon);$$
$$T = t + 273.$$

Where ε is the equivalent strain, $\dot{\varepsilon}$ is the equivalent strain rate, and t is the rolling temperature. The drive spindles contain the torque transducers while the roll separating forces are measured by two force transducers, located under bearing blocks of the bottom roll.

4. Results and discussion

The roll torque and separating force for the above rolling passes are calculated by Eq. (30). The results are compared with the measured ones, as shown in Figs. 2 and 3. The results show that the calculated roll torques and roll separating forces are in good agreement with the actual measured ones; the maximum error percentage is less than 15%. As for the reason why the calculated results of No. 3, No. 8 and No. 9 passes are less than the measured ones, it may attribute to the instability of the deformation resistance model. Besides, it should be pointed out that the calculated roll torque and roll separating force increase slightly when the effect of roll flattening on the roll torque and roll separating force is taken into account. The reason can be attributed to the increase of the equivalent roll radius compared with that of the rigid roll.

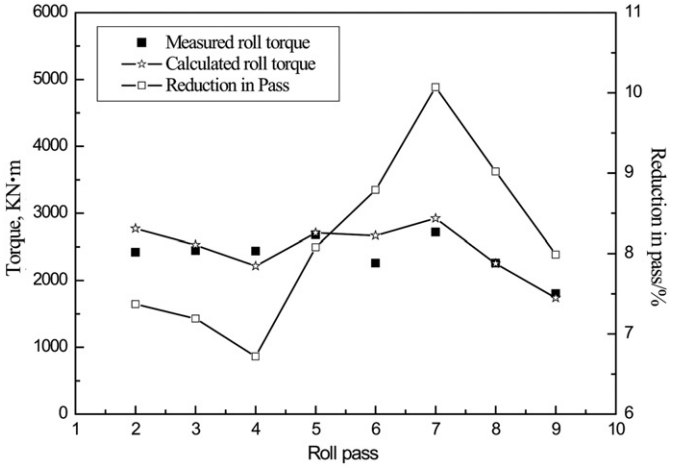

Fig. 2. Comparison between measured and calculated roll torque.

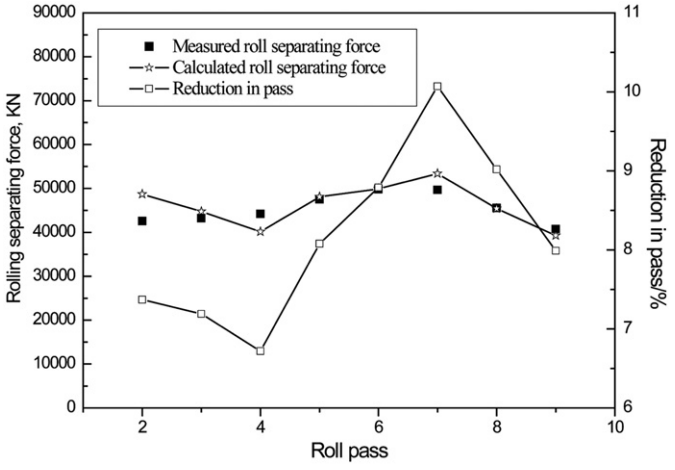

Fig. 3. Comparison between measured and calculated roll separating force.

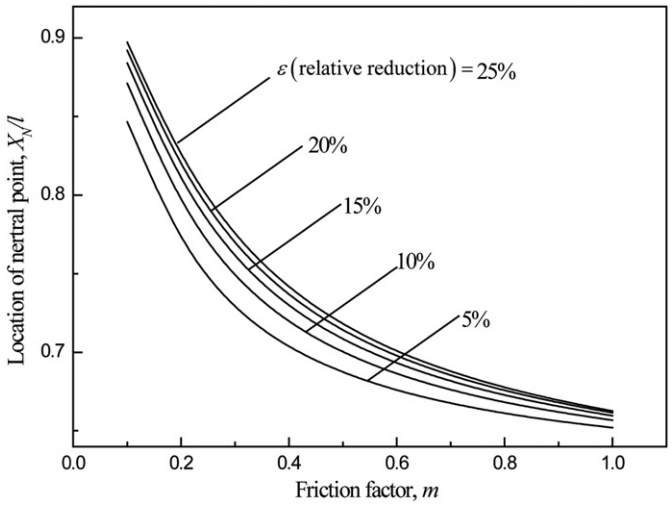

Fig. 4. Effect of m on location of neutral point.

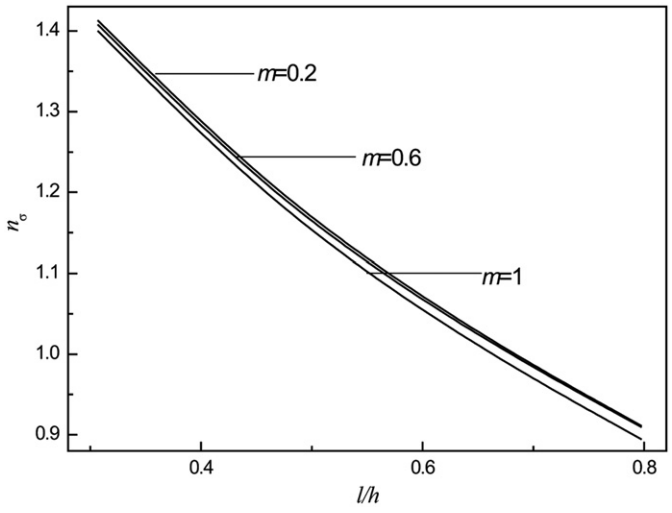

Fig. 5. Effect of l/h on n_σ.

Fig. 4 shows the locations of neutral points as functions of friction factor m for various reductions in thickness. With decreasing friction, the neutral point moves toward the exit plane. Moreover, a small change in friction results in a large change in the neutral point location for$x_n/l \geq 0.75$. The rolling process may become unstable for this range of friction.

Fig. 5 displays the stress state coefficient n_σ as a function of the shape factor. It can be seen that the n_σ increases as the l/h decreases. Although the n_σ reaches its minimum values at $m=1$, the effect of m on n_σ is very litter. The reason is that the friction energy rate is relatively small compared to the plastic deformation energy rate and the shear energy rate for thick plate ($l/h \leq 1$) hot rolling adopted in the present paper. For this reason, the friction factor does not play an important role in n_σ.

5. Conclusions

1. A two-dimensional velocity field deduced by reducing the traditional dual-stream function three-dimensional velocity also satisfies kinematically admissible condition, and is successfully used in analysis of broadside rolling for extra-thick plates.
2. The strain rate vector inner product is first used in analysis of roll separating force during broadside rolling, where spread in longitudinal direction of the slab is negligible, and an analytical solution is first obtained.
3. Comparing the calculated rolling force and roll torque by the solution with measured ones shows a good agreement, and their relative errors are less than 15%.
4. The neutral point moves toward the exit with decrease in friction factor m or increase in reduction ε.
5. The stress factor n_σ increases as the l/h decreases, and the effect of friction factor m is negligible.

Acknowledgements

The authors wish to acknowledge the financial support received from the State Key Laboratory of Rolling and Automation, Northeastern University, China, under the National Natural Science Foundation of China (Grant No. 51074052, 50734002) and the Fundamental Research Funds for the Central Universities (N110607002).

References

[1] Oh SI, Kobayashi S. An approximate method for a three-dimensional analysis of rolling. Int J Mech Sci 1975;17:293–305.
[2] Li GJ, Kobayashi S. Numerical Analysis of Forming Processes. New York: John Wiley and Sons Ltd; 1984.
[3] Kobayashi S. Metal Forming and the Finite Element Method. Oxford: Oxford University Press; 1989.
[4] Park JJ, Oh SI. Application of three dimensional finite element analysis to shape rolling processes. ASME J Eng Ind 1990;112:34–46.
[5] Kim N, Kobayashi S, Altan T. Three-dimensional analysis and computer simulation of shape rolling by the finite and slab element method. Int J Mach Tools Manuf 1991;31:553–63.
[6] Dvorkin E, Goldschmit M, Cavaliere M, Amenta P, Stroppiana W. 2D finite element parametric studies of the flat rolling process. J Mater Process Technol 1997;68:99–107.
[7] Abrinia K, Fazlirad A. Investigation of single pass shape rolling using an upper bound method. J Mater Eng Perform 2008;19:541–52.
[8] Sezek S, Aksakal B, Can Y. Analysis of cold and hot plate rolling using dual stream functions. Mater Des 2008;29:584–96.
[9] Arif S, Ramana Malik, Grandhi V. A computational method to predict strip profile in rolling mills. J Mater Process Technol 2008;206:263–74.
[10] Deng W, Zhao DW, Qin XM. Linear integral analysis of bar rough rolling by strain rate vector. J Iron Steel Res Int 2010;17:28–33.
[11] Zhao DW, Wang GD, Liu XH. Surface integral of three-dimensional velocity field for square bar drawing through conical die. Trans. Nonferrous. Met Soc China 1996;6:131–9.
[12] Zhao DW, Du HJ, Wang GJ. An analytical solution for tube sinking by strain rate vector inner-product integration. J Mater Process Technol 2006;209: 408–15.
[13] Zhao DW, Xie YJ, Liu XH. Three-dimensional analysis of rolling by twin shear stress yield criterion. J Iron Steel Res Int 2006;13:21–6.
[14] Harris JN. Mechanical Working of Metals, Theory and Practice.1st edn. Great Britain: A. Wheaton & Co. Ltd., Exeter; 1983.
[15] Chen QJ, Kang YL, Hong HP, Yu H, Wang LM. Simulation of rolling process for wide and thin plate of alloy steel by finite element method. J Plast Eng 2005;12:163–7.